Correlation of Morphological, Dynamic Mechanical, and Thermal Properties in Compatibilized Polypropylene/Ethylene–Vinyl Acetate Copolymer/Organoclay Nanocomposites

Vahabodin Goodarzi,[1] Seyed Hassan Jafari,[1] Hossein Ali Khonakdar,[2] R. Hässler,[3] Uta Reuter[3]

[1]*School of Chemical Engineering, College of Engineering, University of Tehran, P. O. Box: 11155-4563, Tehran, Iran*
[2]*Iran Polymer and Petrochemical Institute, P. O. Box: 14965-115, Tehran, Iran*
[3]*Leibniz Institute of Polymer Research Dresden, Hohe Strasse 6, D-01069, Dresden, Germany*

Received 29 May 2010; accepted 29 November 2010
DOI 10.1002/app.33849
Published online 29 December 2011 in Wiley Online Library (wileyonlinelibrary.com).

ABSTRACT: Compatibilized and noncompatibilized nanocomposites based on polypropylene (PP)/ethylene–vinyl acetate copolymer (EVA) blends, having 75/25 (wt %/wt %) PP/EVA ratio, with different contents of organoclay (OMMT) and maleated polypropylene as compatibilizer were made through a melt-mixing process with a twin-screw microcompounder, and their properties were investigated. X-ray analysis revealed mainly intercalated/partially exfoliated structures for the blend-based nanocomposites. Through a thermodynamic theoretical approach and transmission electron microscopy investigation, it was shown that the OMMT nanoparticles were mainly placed at the EVA phase of the nanocomposites. Also, scanning electron microscopy analysis showed that OMMT acted like a compatibilizer and reduced the average size of the EVA dispersed phase by preventing coalescence. Dynamic mechanical analysis revealed that the addition of OMMT in the presence of the compatibilizer increased both the storage modulus and damping factor of the corresponding blends. The critical interparticle distance of the EVA domains for achieving supertoughening behavior was obtained at about 100 nm. The addition of OMMT led to a significant improvement in the thermal stability of the blends, especially in the presence of the compatibilizer. A correlation between the morphological, dynamic mechanical, and thermal properties was established to determine the best performing composition, in which desirable damping and stiffness and good thermal stability could be achieved. © 2011 Wiley Periodicals, Inc. J Appl Polym Sci 125: 922–934, 2012

Key words: morphology; nanocomposites; polyolefins; structure–property relations

INTRODUCTION

In semicrystalline polymers having relatively high crystalline contents, the viscous part of the viscoelastic behavior is insignificant, especially at low temperatures. Efforts to improve the damping behavior of semicrystalline materials have been carried out since half a century ago. A conventional method to increase the damping is blending with elastomers such as nitrile rubbers,[1] styrene–butadiene rubber,[2] styrene–butadiene–styrene,[3] and ethylene–propylene–diene monomer.[4] Although the introduction of rubbers improves the toughening behavior of such materials to some extent, it has some drawbacks, such as reductions in the tensile strength and tensile modulus. These are attributed to the inherently low mechanical characteristics of elastomers and a weak interfacial adhesion between the matrix and disperse phases.[5,6] To compensate for these drawbacks, recently ternary composites having thermoplastic and elastomeric components reinforced with an inorganic filler were developed.[7] In this type of composite, the resulting morphology has an important effect on the toughening behavior. Many investigations have been done to elucidate the effect of the particle size of the incorporated filler on the toughening behavior of polypropylene (PP).[8,9] Lim et al.[10] used a relatively new type of toughening agent, that is, poly(ethylene-*co*-octene) copolymer, to overcome the low impact resistance of PP, and by adding small amounts of silica nanoparticles to this blend, they increased the modulus, too. Yu et al.[11] studied the effect of organically modified montmorillonite (OMMT) on poly(L-lactide)/poly(ε-caprolactone) nanocomposites and observed a significant improvement in the tensile and dynamic mechanical properties. Recently, many researchers have independently reported the role of OMMT in the decreasing

Correspondence to: S. H. Jafari (shjafari@ut.ac.ir).
Contract grant sponsor: Iranian Nanotechnology Initiative.

dispersed-phase domain size in polymer blends.[12–15] The majority of them interpreted such a role as a physical barrier that stops the coarsening phenomenon.[12] Also, they reported that a good state of dispersion of OMMT nanoparticles strengthens the pinning effect with increasing viscosity which has a significant effect on the minor-phase domain size. Lipatov and coworkers[13,14] demonstrated that the introduction of fillers into a binary polymeric mixture may increase the compatibility. They reported that the total free energy of a blend system should include an interaction parameter of the phases and the filler. Jang et al.[15] investigated the effect of the polarity on the morphology of polymer/clay nanocomposites. They reported that in nanocomposites with a nonpolar matrix, an intercalated structure was not obtained, whereas in the case of a matrix with adequate polarity, an intercalated/partially exfoliated structure was achieved. In PP/OMMT nanocomposites without a compatibilizer [maleated polypropylene (PP-*g*-MA)], an intercalated/exfoliated structure is not attained because nonpolar chains of PP cannot interact with OMMT platelets and, therefore, do not have a tendency to penetrate into OMMT galleries.[16,17] Also, it was reported that in ethylene–vinyl acetate copolymer (EVA)/OMMT nanocomposite systems, the intercalation of OMMT nanoparticles was due to adequate polarity of EVA, which provided good interaction with OMMT.[18] PP is one of the most used commodity plastics because of its good combination of properties, recyclability, and low cost. However, some disadvantages may limit its use, namely, its poor low-temperature impact strength and surface crazing upon repeated flexing. Among the rubbers being used to compensate for its drawbacks, saturated ones, such as EVA, have gained great attention because of their excellent resistance against thermal, thermooxidation, and UV degradations. More recently, inorganic nanoparticles, such as OMMT, have been used as additives to enhance the stiffness of polymer-blend-based nanocomposites.[19,20]

Mehta et al.'s[21] studies of thermoplastic olefin/clay nanocomposites revealed the clay's role in the segregation of the minor phase, which could increase the impact strength. However, the simultaneous enhancement of the stiffness and toughness in a rubber-toughened system seems to be more valuable from a practical point of view. Considering the clay role in increasing toughness and stiffness, one can anticipate that such an interesting goal can be realized by incorporating clay into a rubber-toughened system. In this study, we examined such a role in a more systematic manner in another rubber-toughed system, namely, PP/EVA, which has a polar rubber component. The polar nature of EVA and its interaction with clay may lead to a better synergism of properties. We also tried to determine what the critical interparticle distance (CID) of the EVA domains was for achieving a supertoughening behavior in the presence of the clay particles. In our earlier articles on this system, we reported the nonisothermal crystallization behavior and thermal/thermooxidative degradation of a series of melt-processed PP/EVA/OMMT nanocomposites.[22,23] These series of nanocomposites showed some interesting crystallization and thermal degradation behaviors. Although the OMMT nanoparticles acted as a barrier for PP macromolecular motion, interestingly they increased the overall crystallization rate and shielding degradation. In this study, the role of OMMT and the OMMT/compatibilizer ratio (O/C) on the tailoring of the morphology and their ultimate effects on the dynamic mechanical parameters, such as damping, toughness, and stiffness, and also on the thermal stability of the PP/EVA/OMMT nanocomposites were explored. An attempt was also made to establish correlations among the morphological, dynamic mechanical, and thermal properties.

EXPERIMENTAL

Materials

PP (grade Novolen 1100r) was supplied by Targor Co. (BASF, Ludwigshafen, Germany). EVA (grade Escorene Ultra UL00218CC3, 18 wt % vinyl acetate) was obtained from ExxonMobil Chemical Co., Houston, TX. PP-*g*-MA (grade Polybond 3200) as the compatibilizer was procured from Chemtura Co., Philadelphia, PA. The OMMT used was Nanomer I.44 (Nanocor, Inc., Arlington Heights, IL) modified with the ammonium salt dimethyldialkylammonium halide (70% C18, 26% C16, and 4% C14).[24]

Sample preparation

The blends and blend-based nanocomposites were prepared via a one-step process in a conical twin-screw DACA microcompounder. Before the melt-mixing process, all of the components of the blends or blend-based nanocomposites were dry-premixed at a specified ratio and then fed into the microcompounder. PP/EVA (75/25 w/w) blend-based nanocomposites with 0–7 wt % OMMT and 15 and 7 wt % PP-*g*-MA were made. In addition, the neat components (PP and EVA) were melt-mixed separately with 5 wt % OMMT under similar processing conditions. A processing temperature of 210°C, a screw speed of 150 rpm, and a mixing time of 5 min were used for the preparation of all of the blends and blend-based nanocomposites. The extruded strands, with a length of 2 cm and a diameter of 2 mm, were cooled on an aluminum tray in air. For

TABLE I
Composition of the Samples

Sample code	PP (wt %)	EVA (wt %)	Compatibilizer (PP-*g*-MA; wt %)	OMMT
P100	100	0	0	0
E100	0	100	0	0
P95O5	95	0	0	5
E95O5	0	95	0	5
P75E25	75	25	0	0
P75E25C5	75	25	5	0
P75E25O5	75	25	0	5
P75E25C1O5	75	25	1	5
P75E25C5O5	75	25	5	5
P75E25C7O5	75	25	7	5
P75E25C5O1	75	25	5	1
P75E25C5O7	75	25	5	7

dynamic mechanical analysis (DMA) studies, the extruded strands were compression-molded into rectangular sheets 0.5 mm thick and with dimensions of 20 × 10 mm^2. The molding was performed at a temperature of 210°C and a pressure of 10 MPa. The compositions of the prepared samples are presented in Table I.

Characterization

Wide-angle X-ray diffraction (WAXS) analysis was done with an X-ray diffractometer P4 with an area detection system (GADDS, Siemens AG Karlsruhe, now BRUKER axs Karlsruhe, Germany) operating at 40 kV and 30 mA for Cu Kα radiation (λ = 0.154 nm). The samples were investigated in transmission with the primary beam perpendicular to the plane of the extruded stands. The scattering range was 2θ = 1.8–10°. Intensity (2θ) plots were obtained by sectoral integration (±30° in relation to the extrusion direction) with steps of Δ2θ = 0.1° (mean measuring time = 1200 s). The dispersion of the OMMT platelets in the blend was studied by means of transmission electron microscopy (TEM). Ultrathin sections of the extruded samples (ca. 80 nm thick) were obtained under cryogenic conditions at −120°C with an EM UC/FC6 ultramicrotome (Leica) equipped with a diamond knife. These ultrathin sections were collected on 300-mesh copper TEM grids, and they were investigated by means of a LEO 910 TEM instrument (Carl Zeiss) at an accelerated voltage of 120 kV. The sections were not stained because the EVA phase would then become too dark for the identification of clay nanoparticles in a descriptive way. The chance to see a good difference between PP, EVA, and the OMMT nanoparticles without staining was very high.

Scanning electron microscopy (SEM) was used to characterize the morphology of the blends and blend-based nanocomposites. An extruded polymer strand was immersed in liquid nitrogen for some time, and a brittle fracture was performed. The fractured surface was etched in 1,2-dichloroethane for 1.5 h to remove the EVA phase of the samples. The etched surfaces after proper drying were gold-sputtered and observed under a Philips CM200 SEM instrument. With image analysis software of the SEM instrument, the number-average particle size (D_n), weight-average particle size (D_w), volume-average particle size (D_v), standard deviation (S_n), and dispersed particle density (λ_n) were calculated by means of the following equations:

$$D_n = \sum N_i D_i \Big/ \sum N_i \tag{1}$$

$$D_w = \sum N_i D_i^2 \Big/ \sum N_i D_i \tag{2}$$

$$D_v = \sum N_i D_i^3 \Big/ \sum N_i D_i^2 \tag{3}$$

$$S_n = \left[\frac{1}{n}\sum (D_i - D_n)^2\right]^{0.5} \tag{4}$$

$$\lambda_n = \left(\frac{n}{A}\right) \times 10^6 \tag{5}$$

where N_i is the number of domains in a determined range of diameters, D_i is the diameter of domains, n is the total number of domains, and A is the scanned area. The ratio of the interlayer area (A_{3D}) to the unit volume of the dispersed phase (V_{3D}) could be calculated from the total domains perimeter (P_{2D}) divided by total domains area (A_{2D}) obtained from the SEM images with the following equation:

$$A_i\left(\mu m^2/\mu m^3\right) = P_{2D}/A_{2D} = A_{3D}/V_{3D} \tag{6}$$

The interparticle distance (ζ) in the continuous phase was calculated on the basis of Wu's[25] equation:

$$\varsigma = D_n\left\{\left[\left(\frac{\pi}{6\phi_d}\right)\right]^{1/3} - 1\right\} \tag{7}$$

where ϕ_d is the volume fraction of the domain phase. DMA was performed by means of a DMA2980 (TA Instruments) into bending mode with a single-cantilever clamp with frequency of 10 Hz, a temperature range of −150 to 150°C, and a heating rate of 3 K/min on the compression-molded samples with dimensions of 20 × 10 × 0.5 mm^3. Thermal degradation was investigated with a Q500 thermogravimetric analyzer (TA Instruments). The analysis was performed under an air atmosphere with a flow rate of 60 mL/min and within the temperature of range 30–700°C with a programmed heating rate of 10 K/min.

Most of the analyses were done on the extruded strands, whereas the DMA test was performed on

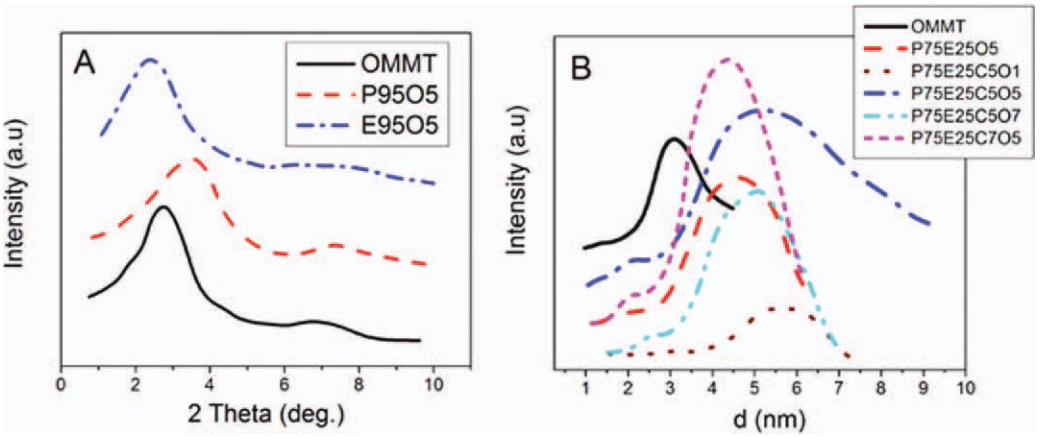

Figure 1 WAXS patterns of the (A) reference materials in terms of intensity versus 2θ and (B) PP/EVA/compatibilizer/OMMT nanocomposites in terms of intensity versus *d*-spacing. [Color figure can be viewed in the online issue, which is available at wileyonlinelibrary.com.]

the molded samples because samples with exact dimensions were needed for the DMA test. Our hypothesis is that the morphology remained stable because, during the compression-molding process, the samples did not experience rigorous shearing or elongational melt flow as of the extrusion process.

RESULTS AND DISCUSSION

WAXS analysis

The WAXS patterns of the neat OMMT, PP/OMMT, 95/5 wt/wt (P95O5), and EVA/OMMT, 95/5 wt/wt (E95O5), as reference materials, in terms of intensity versus 2θ are presented in Figure 1(A), whereas the related WAXS patterns of the nanocomposites, in terms of intensity versus *d*-spacing (nm), are shown in Figure 1(B). Because our aim was to clearly show the influence of each component on the nanocomposite microstructure, the X-ray diffraction patterns of the main systems are presented in terms of the intensity versus *d*-spacing. In this way, small changes in the *d*-spacing can be traced in a clearer way. These patterns were analyzed quantitatively, and the *d*-spacing values are presented in Table II. From this table, one can see that the P95O5 sample has the minimum interlayer spacing. This is attributed to an exerted repulsive force between the PP chains and OMMT layers due to the difference in their polarities. This force reduces the OMMT interlayer spacing. Therefore, the PP chains could not diffuse into the gap between the OMMT platelets.[26] For the EVA/OMMT sample, the interlayer spacing increased and resulted in an intercalated structure. This indicated a better interaction between the EVA matrix and OMMT nanoparticles, probably due to the higher polarity of EVA, which had polar side groups, compared to PP. The greater interlayer spacing of P75E25O5 compared to that of P95O5 was more evidence for a better diffusion of EVA chains into the clay galleries.

The highest d_{001}-spacing was observed for the P75E25C5O1 sample. The addition of PP-*g*-MA decreased the interfacial tension between PP and EVA and increased the chances of the interaction of PP and EVA macromolecules with OMMT platelets and facilitated the diffusion of PP and EVA chains into the OMMT galleries.[27,28]

The data shown in Figure 1 and Table II demonstrated that the interlayer spacing of the OMMT denoted as P95O5 for the different blend-based nanocomposites was highly dependent on O/C. With decreasing of this ratio, the *d*-spacing increased; this implied that the compatibilizer played an important role in the intercalation process.

Morphological analysis

The balanced situation of OMMT nanoparticles in blend-based system was determined by the thermodynamics of the system. The dispersion state of OMMT nanoparticles in a polymer matrix is generally in two forms: (1) the particles are dispersed uniformly in one of the phases, or (2) the particles are placed at the interface of the two phases. The

TABLE II
Data Obtained from X-Ray Diffraction Analysis for Various Samples

d_{001} (nm)	Sample
3.07	OMMT
2.42	P95O5
4.32	E95O5
4.54	P75E25O5
5.07	P75E25C5O5
5.73	P75E25C5O1
4.91	P75E25C5O7
4.41	P75E25C7O5

TABLE III
Surface Energy Data for the Reference Materials

Sample	Surface tension at 25°C (mN/m)			Polarity	Surface tension at 210°C (mN/m)			Polarity
	γ	γ^d	γ^p	(γ^p/γ)	γ	γ^d	γ^p	(γ^p/γ)
PP	30.0	26.0	4.0	0.13	20.6	17.9	2.8	0.13
EVA	37.2	29.7	7.5	0.20	25.6	20.44	5.16	0.20
OMMT	48.4	27.6	20.8	0.43	30.2	17.2	13.0	0.43

occurrence of either of these states depends on the surface energy of the individual components. To determine the state of OMMT localization in a blend-based nanocomposite system, the following theoretical approach based on the wetting parameter (Δ_i) can be used:[29]

$$\Delta_i = \frac{\gamma_{\text{Clay}-2} - \gamma_{\text{Clay}-1}}{\gamma_{12}} \tag{8}$$

where $\gamma_{\text{Clay}-i}$ is the interfacial tension between the OMMT layers and polymer component i and γ_{12} is the interfacial tension between the two polymer components. According to eq. (8), when $\Delta_i > 1$, the OMMT layers are only in the polymeric phase 1, and when $\Delta_i < -1$, the OMMT nanoparticles are only in polymeric phase 2. If the value is between -1 and 1, the OMMT layers are at the interface. γ_{12} can be calculated on the basis of Wu's[30] equation:

$$\gamma_{12} = \gamma_1 + \gamma_2 - \frac{4\gamma_1^d\gamma_2^d}{\gamma_1^d + \gamma_2^d} - \frac{4\gamma_1^d\gamma_2^d}{\gamma_1^d + \gamma_2^d} \tag{9}$$

where γ_i is the surface energy of a material, and the superscripts p and d represent the polar and dispersive contributions of the surface energy, respectively.

The surface energy at a desired temperature [T (K)] can be calculated with the relative Guggenheim[31] equation:

$$\frac{\gamma_x}{\gamma_y} = \left(\frac{T_{Cr} - T_x}{T_{Cr} - T_y}\right)^{\frac{11}{9}} \tag{10}$$

where γ_x and γ_y are the surface energies at temperatures T_x and T_y, respectively, and T_{Cr} is the critical temperature. T_{Cr} is defined as the temperature at which the interfacial surface between a liquid and gas is eliminated. In these calculations, it is assumed that all of the components have the same dependency on temperature.

The surface energies of PP, EVA, and OMMT and the value of T_{Cr} (1000 K) were obtained from the literature[32,33] and then shifted to 210°C with eq. (10). These values are presented in Table III. Using these data and on the basis of eq. (9), we calculated the values of interfacial tension at 210°C for PP/EVA, PP/OMMT, and EVA/OMMT to be 0.90, 6.66, and 3.64 mJ/m^2, respectively. When we considered these data and used eq. (8), the Δ_i for PP/EVA/OMMT system became $\Delta_i = 3.34$, which indicated that the OMMT nanoparticles were localized in the EVA phase.

The work of adhesion (W_{AB}) can be calculated according to the following equation:[34]

$$W_{AB} = 2\left(\gamma_1^d\gamma_2^d\right)^{1/2} + 2\left(\gamma_1^p\gamma_2^p\right)^{1/2} \tag{11}$$

Using this equation, we found the values of W_{AB} for PP/EVA, PP/OMMT, and EVA/OMMT to be 45.78, 47.04, and 53.87 mJ/m^2, respectively. The high interfacial tension, along with the low value of W_{AB}, obtained for PP/OMMT was an indication of incompatibility between PP and OMMT.

TEM and SEM analysis

The cryofractured surface morphologies of the P75E25, P75E25C5, and P75E25O5 samples are shown in Figure 2(A–C). In these SEM images, the etched EVA phase appears as dark domains. Generally, the incorporation of the compatibilizer and

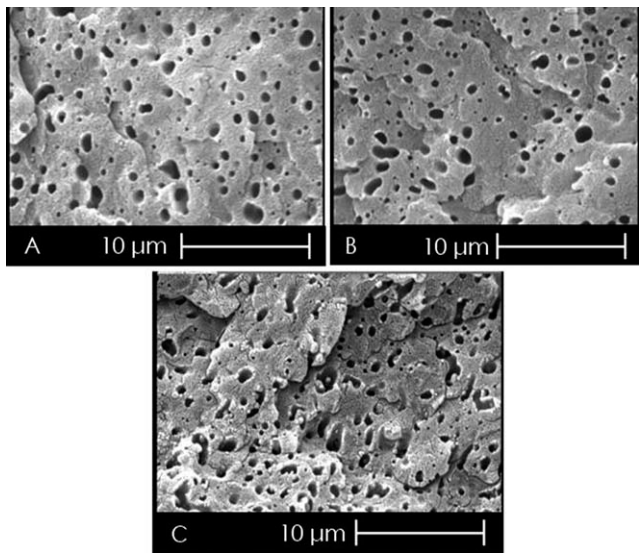

Figure 2 SEM photomicrographs of (A) P75E25, (B) P75E25C5, and (C) P75E25O5.

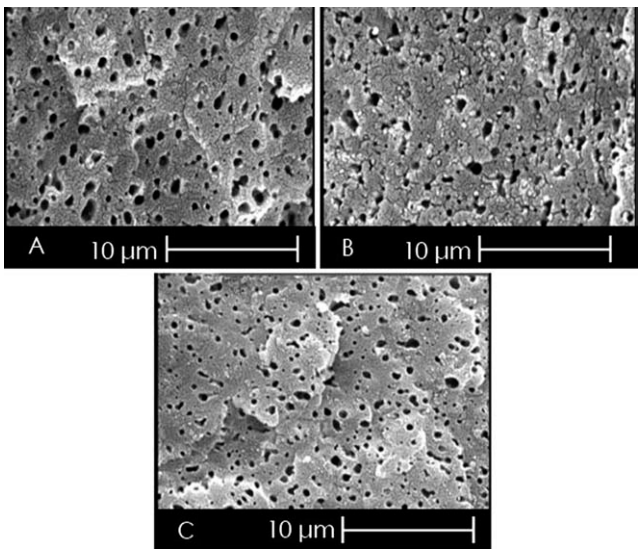

Figure 3 SEM photomicrographs of (A) P75E25C5O1, (B) P75E25C5O5, and (C) P75E25C7O5.

OMMT decreased the average size of EVA domains and also the roughness at the interface of polymer pairs; this indicated an enhancement in the interfacial adhesion and an improvement in the compatibility.[35] This implied that the OMMT nanoparticles, with their highly active surface, acted as an effective barrier against coalescence in this system. As shown in Figure 3(A), the incorporation of a higher amount of OMMT (5 wt %) into the compatibilized PP/EVA system with 5 wt % compatibilizer slightly reduced the average EVA domain size [cf. Fig. 3(A) with Fig. 3(B)]; also, this reduction was more pronounced in the presence of a higher amount (7 wt %) of compatibilizer [cf. Fig. 3(A) with Fig. 3(C)].

Quantitative analyses of these SEM images were done, and the results are presented in Table IV. From the obtained data, we observed that the incorporation of OMMT decreased the EVA domain size. This could be attributed to the tendency of OMMT toward being localized in the EVA phase. This increased viscosity of the EVA phase, in turn, impeded the coalescence phenomenon.[22,23] Also, the addition of OMMT increased the number density of EVA domains; this, in turn, decreased the average distance between the EVA domains. The histograms showing the particle size distributions are shown in Figure 4. The histograms illustrate the EVA domain size distribution in the PP matrix. Generally, the addition of OMMT and the compatibilizer decreased the EVA domain size and provided a uniform domain size distribution. Also, the number of EVA domains increased as a result of the decreased domain size. From these histograms, it was clear that the P75E25C5O5 sample had the narrowest EVA domain size distribution in the PP matrix. This showed that the proper balance between the OMMT and compatibilizer contents could lead to the development of nanocomposite systems with desired morphologies. This effect of O/C on the properties of the nanocomposites is discussed in the subsequent section.

TEM images of the PP/EVA blend-based nanocomposites are shown in Figure 5(A–C). The dark regions represent EVA irregular domains dispersed in the light PP matrix. In the case of the P75E25C5O1 sample [Fig. 5(A)], which had a low OMMT content, the OMMT nanoparticles were mainly seen within the EVA phase, and in some cases, they were on the surface of the EVA domains. They had an intercalated/partially exfoliated state of dispersion. This higher tendency of OMMT toward the EVA phase was due to the relatively higher polarity of EVA compared to that of PP. Figure 5(B,C) shows the dispersion state of OMMT in the presence of high amounts of compatibilizer and OMMT. With the addition of the compatibilizer, the OMMT nanoparticles tended to be localized at the interface, showing an intercalated structure [Fig. 5(B)]. However, when, in the same system, the compatibilizer content was reduced, they again showed some tendency toward EVA domains [Fig. 5(C)]. The introduction of the compatibilizer to the system not only increased the compatibility of the PP and EVA phases, but it also increased the interaction between the OMMT and PP phase. Thus, in the absence of compatibilizer, the OMMT nanoparticles did not show good

TABLE IV
Data Obtained from SEM Analysis

Sample	D_n (μm)	D_w (μm)	D_v (μm)	A (μm^2/μm^3)	S_i (μm)	λ_n (μm)$^{-2}$	ζ (μm)
P75E25	1.2	1.3	1.6	0.3	0.30	0.03	0.3
P75E25C5	0.7	1.2	1.4	3.7	0.26	0.06	0.2
P75E25O5	1.1	1.3	1.5	4.1	0.18	0.08	0.3
P75E25C5O5	0.3	0.5	0.5	14.4	0.06	0.06	0.1
P75E25C1O5	1.1	1.2	1.2	5.1	0.16	0.06	0.3
P75E25C7O5	0.3	0.4	0.5	15.3	0.04	0.07	0.1
P75E25C5O1	0.6	0.7	0.7	8.3	0.06	0.05	0.2
P75E25C5O7	0.4	0.5	0.5	15.2	0.15	0.07	0.1

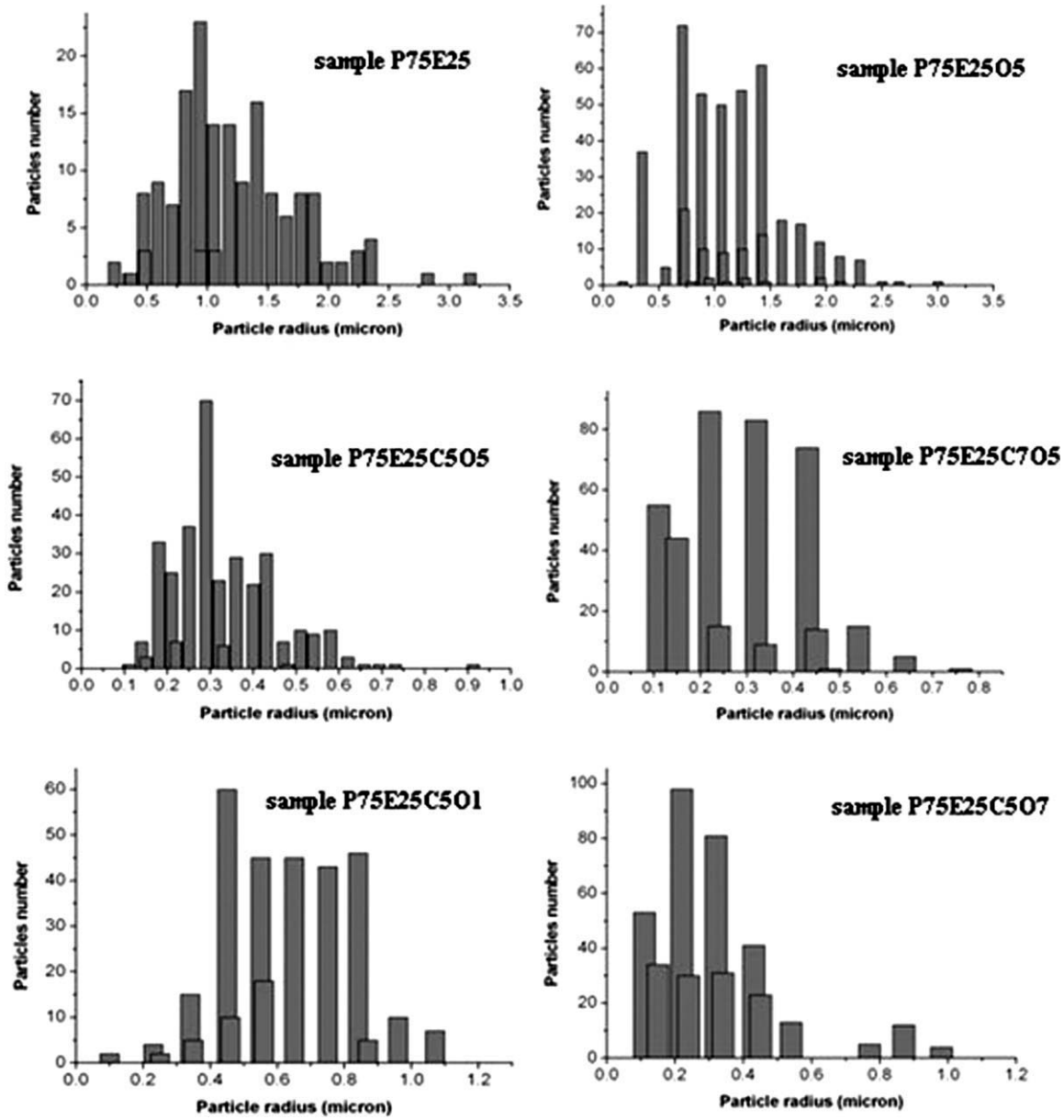

Figure 4 Histograms demonstrating the EVA domain size distributions in different PP/EVA blend-based nanocomposites.

interaction with the PP chains and, hence, were localized in the EVA phase.

The role of OMMT in the prevention of coalescence in the immiscible polymer blend and the reduction of the dispersed-phase domain size was attributed mainly to the OMMT localization at the polymer/polymer interface; this could have a role very similar to a block copolymer. The reduction of the interfacial tension due to the distribution of the OMMT platelets at the polymer/polymer interface could be a reasonable explanation for the compatibilization. The modification of the interfacial tension affected the breakup/coalescence equilibrium in favor of the breakup; this could have led to smaller drops. On the other hand, the refinement of the morphology due to the localization of OMMT in a more polar blend component, which formed the dispersed phase, could be attributed to changes in the rheological characteristics of the system, such as the elasticity and viscosity ratio, that could control the morphological evolution. One should not forget that there was also a relatively rare possibility for OMMT to increase the dispersed-phase domain size during blending by a combination of changes in the interfacial and rheological effects. In such cases, the breakup/coalescence equilibrium is more in favor of coalescence. Recently, different mechanisms for changes in the interfacial tension due to the dispersion of OMMT layers in immiscible polymer blends have been

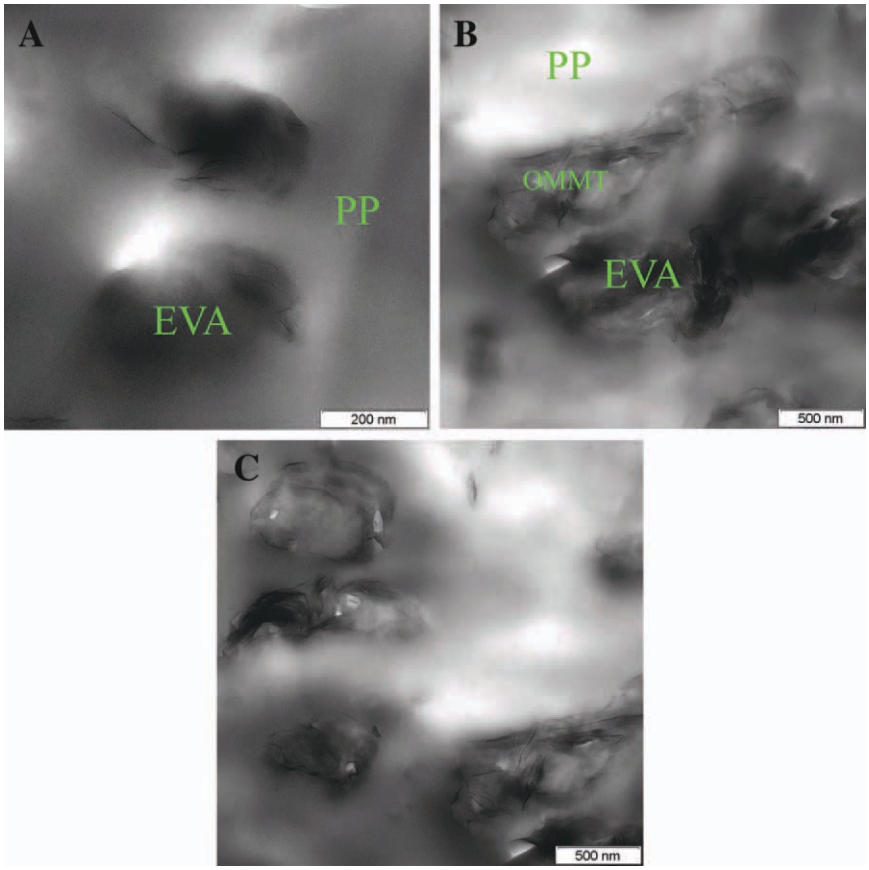

Figure 5 TEM images of the PP/EVA blend-based nanocomposites: (A) P75E25C5O1, (B) P75E25C5O5, and (C) P75E25C7O5. [Color figure can be viewed in the online issue, which is available at wileyonlinelibrary.com.]

discussed extensively by Fenouillot et al.[36] and Liu et al.[37]

DMA

Figure 6(A) depicts the changes in the storage modulus of different samples against temperature. All of the samples showed the maximum modulus in the glassy region. The addition of EVA to PP decreased the modulus compared to that of neat PP. This decrease in the modulus was attributed to the presence of a low-modulus EVA phase, which had some hindering effect on the crystallization of PP, too. In our previous study,[22] we observed that when EVA was incorporated into the PP matrix, the final degree of crystallinity of PP dropped by nearly 15%; however, EVA had almost no effect on the crystalline structure of PP, and hence, PP crystallized in its original α-crystalline form. The incorporation of 5 wt % PP-*g*-MA did not change the storage modulus significantly, whereas with the introduction of 5 wt % OMMT, the storage modulus increased to some extent. When 5 wt % OMMT was added in the presence of 5 wt % PP-*g*-MA, a stronger influence was seen on the storage modulus. This confirmed the synergistic role of the OMMT layers in strengthening the interface when combined with the compatibilizer. Increasing the compatibilizer loading to 7 wt % increased the storage modulus even further. The highest storage modulus was observed in the sample loaded with 7 wt % OMMT in the presence of 5 wt % compatibilizer. Interestingly, the highest refinement of morphology was observed for this sample, too. Almost the same trend of variation in the storage modulus was seen above the glass-transition temperature of PP (~ 20°C), but the differences between samples became much less. The improvement in the storage modulus in the presence of OMMT layers was due to their large aspect ratio. These nanoparticles impeded the segmental motion of the polymeric chains and, thus, increased the chain stiffness. Figure 6(B) shows the loss factor (tan δ) versus temperature curves for different samples. Four relaxation peaks were distinguishable. The presence of individual β transitions, which were related to the glass-transition temperature of each polymer pair, showed that the PP/EVA blends were immiscible. The introduction of OMMT and compatibilizer shifted the relaxation peaks and altered the viscoelastic behavior of the samples. The results of a quantitative analysis on these tan δ curves are summarized in Table V. The addition of OMMT and

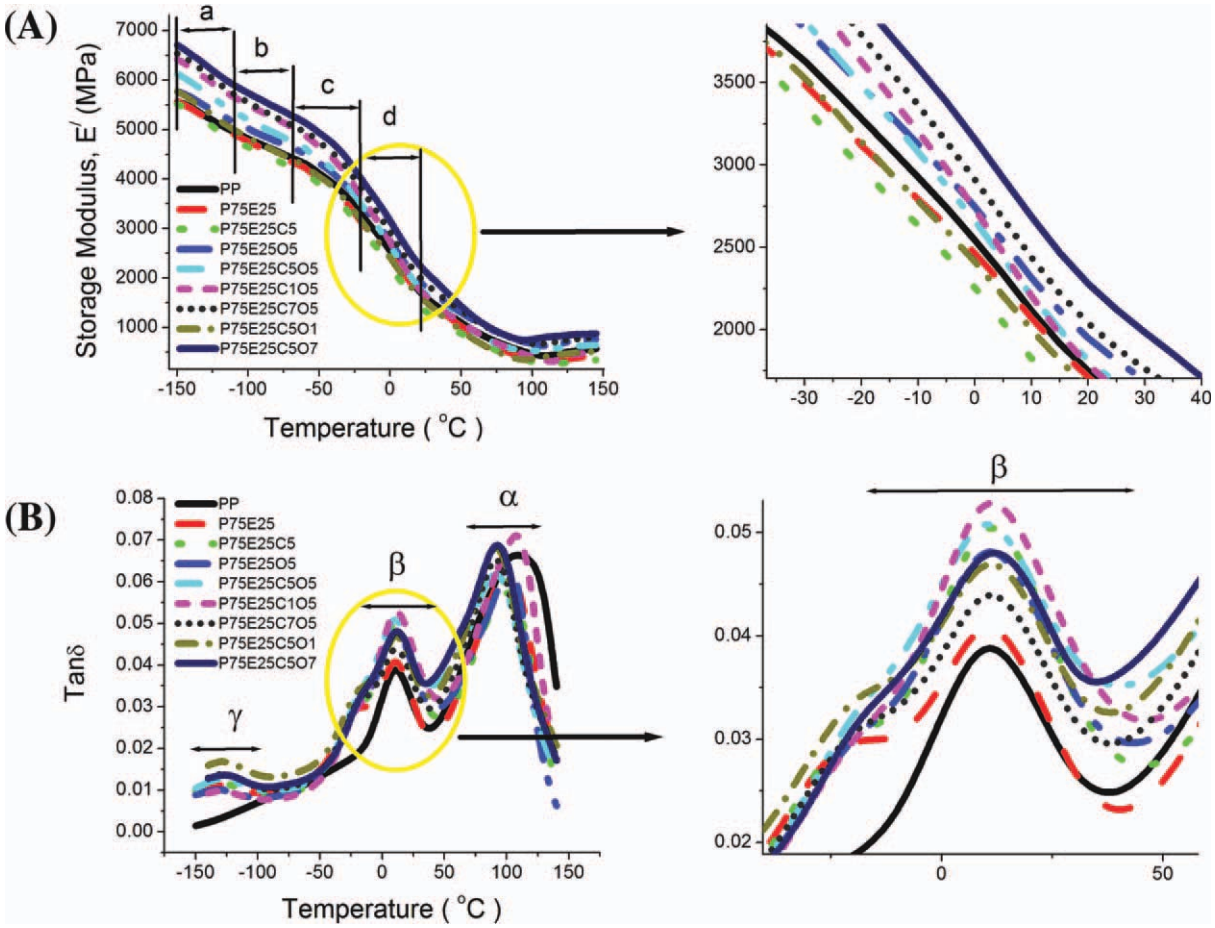

Figure 6 DMA curves for the PP/EVA blend-based nanocomposites: (A) storage modulus and (B) tan δ. [Color figure can be viewed in the online issue, which is available at wileyonlinelibrary.com.]

compatibilizer to the blend did not show a significant and systematic effect on the β transition of the PP phase. However, it reduced the α-transition temperature to some extent. In the case of the EVA phase, the inclusion of OMMT nanoparticles and compatibilizer resulted in the dislocation of the β transition to lower temperatures but did not show a significant effect on the γ transition. Such an effect was reported previously by Feng et al.[38] in a PP/PA6 blend-based nanocomposite system. A correlation between ζ of the EVA domains in the PP matrix (see Table IV) and the total loss peak area (as an

TABLE V
DMA Data of the Prepared Samples

Sample	Transition temperature of PP (°C)		Transition temperature of EVA (°C)		Loss peak area (arbitrary units)	Total loss peak area (arbitrary units)
	T_β	T_α	T_γ	T_β		
PP	11	110	—	—	—	7.45
P75E25	10	103	−129	−21	5.97	8.00
P75E25C5	10.7	102	−131	−20	6.02	8.04
P75E25O5	12	98	−130	−22	6.25	8.10
P75E25C5O5	10	93	−128	−18	6.56	8.60
P75E25C1O5	10.2	105	−130	−19	6.62	8.08
P75E25C7O5	11	98	−128	−18.5	7.02	9.19
P75E25C5O1	10	91	−131	−20	6.20	8.17
P75E25C5O7	12	92	−130	−17	6.83	9.10

T_α is α transition temperature.
T_β is β transition temperature.
T_γ is γ transition temperature.

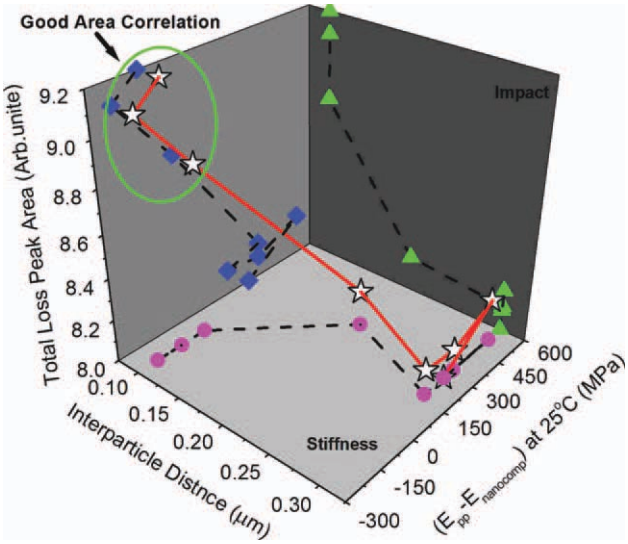

Figure 7 Interrelation between ζ of the EVA domains, total loss peak area, and different storage moduli between PP and the PP/EVA blend-based nanocomposites. E_{PP} and $E_{nanocomposite}$ are modulues of neat and nanocomposite, respectively. [Color figure can be viewed in the online issue, which is available at wileyonlinelibrary.com.]

assessment of the viscoelastic properties; Table V), as well as differences between the storage modulus of PP and those of other samples at 25°C, is presented in Figure 7. The observed trend was similar to that of the notched Izod impact strength versus ζ of rubber particles, which is employed to obtain CID.[39] This critical value is used to probe supertoughening phenomenon.[40] On the other hand, the area under the peak of tan δ can be used to judge the impact strength.[41] As shown in Figure 7, the CID in this case was about 100 nm. ζ beyond this value resulted in a decrease of ductility and toughness. Also, a large modulus difference between PP and other nanocomposite samples was observed at the CID. It was interesting that there were simultaneous increases in the toughness and modulus, regardless of OMMT dispersion, in the PP/EVA/clay nanocomposite systems. This could be explained on the basis of the fact that the particle size, rubber ζ, rubber-to-matrix modulus ratio, and Poisson's ratio are known to be effective parameters on the toughness of rubber-toughened polymer blends.[39] In the studied systems, we observed that the average EVA domain size and EVA ζ were reduced; this could have affected the toughness. On the other hand, the localization of relatively stiff OMMT platelets in the EVA phase increased its modulus. Therefore, enhancements in both the stiffness and toughness were observed. A similar phenomenon was also reported in the toughening of unsaturated polyester resins, in which its stiffness increased simultaneously.[42] Supertoughness behavior was observed in a PP/PP-*g*-MA/poly(ethylene-*co*-octene)/montmorillonite system by Lee et al.[43] They explained this interesting behavior by the morphological change in the presence of the filler, which reduced the size of the elastomer domains to less than 1 μm.

Figure 8(A) illustrates a correlation among a relative factor used for the evaluation of the extent of chain mobility in the presence and absence of a filler (C_β; %), total loss peak area, and O/C. The relative extent of chain mobility for each phase in the PP/EVA system loaded with both OMMT and compatibilizer with respect to the neat blend could be expressed as follows:

$$C_\beta(\%) = \left(\frac{\tan\delta'_\beta - \tan\delta_\beta}{\tan\delta_\beta}\right) \times 100 \qquad (12)$$

where $\tan\delta_\beta$ is the loss factor of each component in the neat blend and $\tan\delta'_\beta$ is the corresponding loss factor value in the nanocomposite system. As

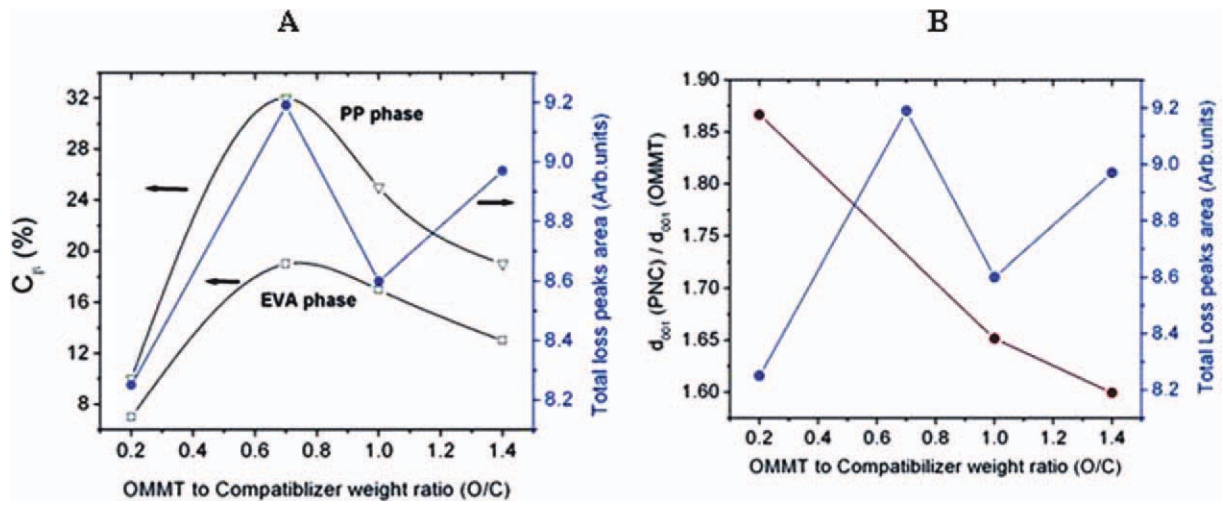

Figure 8 Interrelation between (A) C_β (%) and (B) *d*-spacing with total loss peak area and O/C in the PP/EVA blend-based nanocomposites. [Color figure can be viewed in the online issue, which is available at wileyonlinelibrary.com.]

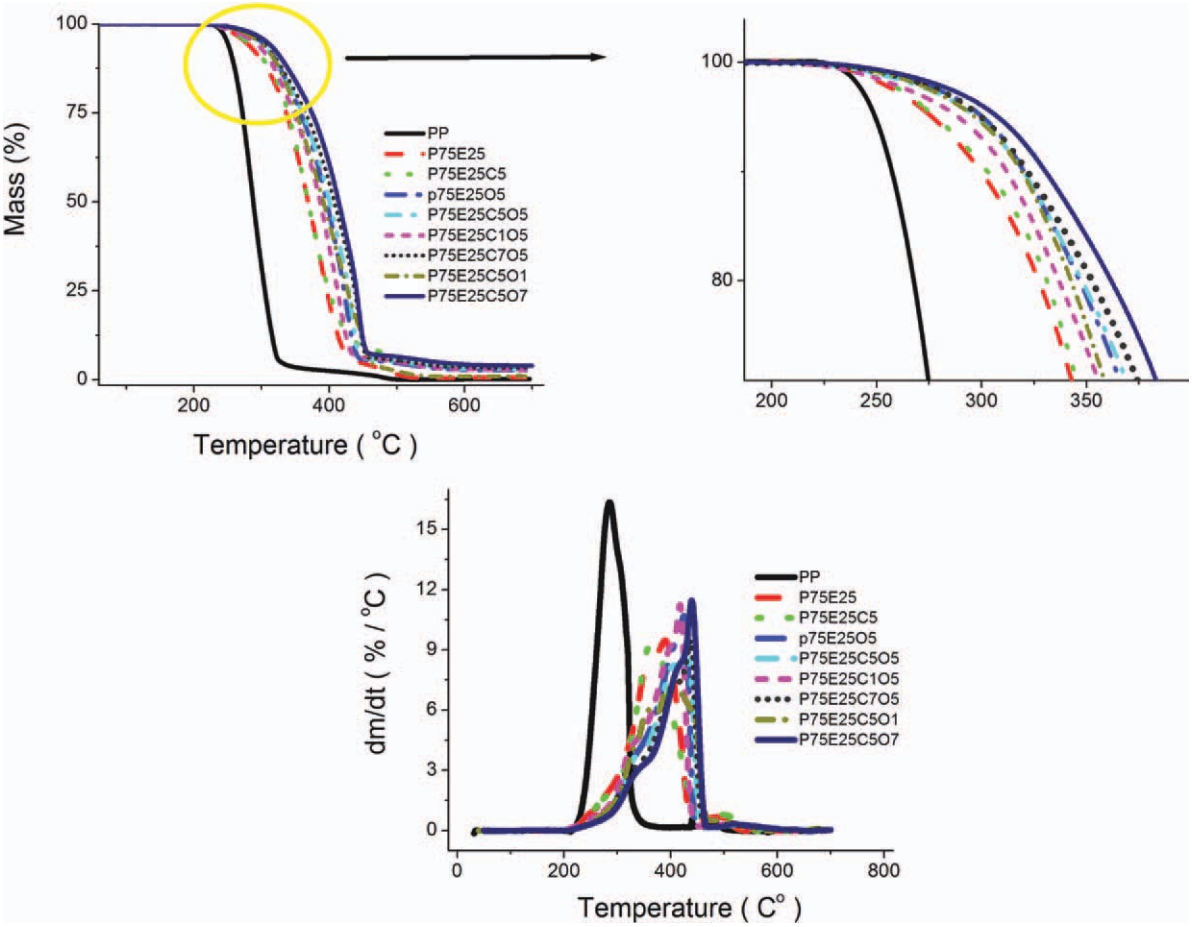

Figure 9 TGA and DTG thermograms of the PP/EVA blend-based nanocomposites. dm/dt is the rate of mass change with time. [Color figure can be viewed in the online issue, which is available at wileyonlinelibrary.com.]

shown in Figure 8(A), primarily, an increase in the O/C ratio to some level facilitated the mobility of both PP and the EVA chains in the nanocomposites in comparison to the P75E25 blend. This effect was more pronounced for PP compared to the EVA phase. This was attributed to the higher tendency of OMMT nanoparticles to move toward the EVA phase than toward PP. Above a certain level of O/C, the chain mobility was hindered. The hindrance effect at high O/C ratios was possibly due to the network formation of OMMT species analogous to a physically crosslinked network. According to Kade and Padden's theory,[44] a high inclusion of OMMT results in a pronounced defect in crystalline structures. This accordingly increased the amorphous regions and resulted in an increase in damping. As shown in Figure 8(B), the highest *d*-spacing corresponded to the lowest toughness because a higher amount of macromolecular chains were engaged in the gaps between the OMMT layers. On the other hand, increasing the OMMT content at constant compatibilizer inclusion impeded the diffusion of polymer chains into the gallery spacing. Hence, *d*-spacing decreased, and the polymer chain mobility did not decrease. Using the data presented in Figure 8(B), we established a relationship by applying nonlinear regression between the gallery spacing of OMMT in the blend-based nanocomposites and O/C as follows:

$$\frac{(d_{001})_{\text{nanocomposite}}}{(d_{001})_{\text{OMMT}}} = 1.65\left[\frac{(\text{wt\%})_{\text{OMMT}}}{(\text{wt\%})_{\text{compatibilizer}}}\right]^{-0.077} \quad (13)$$

Also, the addition of OMMT probably promoted the development of defects within the crystalline regions and, hence, increased the amorphous regions. This resulted in an increase in the toughness of the system.

Thermogravimetric analysis (TGA)

Using OMMT nanoparticles in polymer matrices, according to two main mechanisms of barrier and free-radical trapping, improved the thermal stability of the blend-based nanocomposites.[23,45] The TGA thermograms of the PP/EVA blend-based nanocomposites and the neat components are shown in

TABLE VI
TGA Data of the Prepared Samples

Sample	$T_{5wt\%}$ (°C)	$T_{10wt\%}$ (°C)	$T_{50wt\%}$ (°C)	T_{max} (°C)	Char yield at 400°C	Char residue (%)
PP	249	257	288	284	2.37	0.02
P75E25	275	299	368	389	21.7	0.66
P75E25C5	279	301	368	362	23.6	0.72
P75E25O5	299	321	397	430	47.4	2.73
P75E25C1O5	288	312	387	419	37.2	2.81
P75E25C5O5	298	319	399	431	50.7	2.96
P75E25C7O5	300	322	407	440	56.0	3.26
P75E25C5O1	291	318	391	391	44.4	1.01
P75E25C5O7	308	324	410	441	58.0	4.23

*T_{10}wt% and T_{50}wt% are temperatures at 10 wt% and 50 wt% weight loss, respectively. T_{max} is the temperature at which the maximum rate of degradation are seen.

Figure 9, and related data are presented in Table VI. A more thermally stable EVA phase increased the thermal stability of PP significantly. The addition of OMMT to this blend system increased the stability further. The onset of degradation temperature ($T_{5wt\%}$) for all of the samples containing OMMT was nearly 50°C higher than that of the neat PP. This indicated a strong shielding effect of OMMT in prevention of the degradation. The compatibilizer/OMMT (C/O) ratio played a role in the improvement of the thermal stability, too. A comparison between the P75E25C5O1 and P75E25C5O7 samples showed that an increase in C/O enhanced the thermal characteristics of the nanocomposites. Figure 10 illustrates the correlations among the morphology, tan δ, and TGA results. As shown, the average particle size of the dispersed phase had a significant influence on the total loss peak area and the thermal stability of the system; the lower the average particle size was, the higher the thermal stability was, and the higher the loss peak area was.[23] The decrease in the EVA average particle size increased the interfacial area and also the number of dispersed particles in the matrix. With the higher thermal stability of EVA compared to PP and the fact that OMMT particles were mainly in the EVA phase, as discussed earlier, the improvement in the thermal stability of the blend-based nanocomposites could be explained.

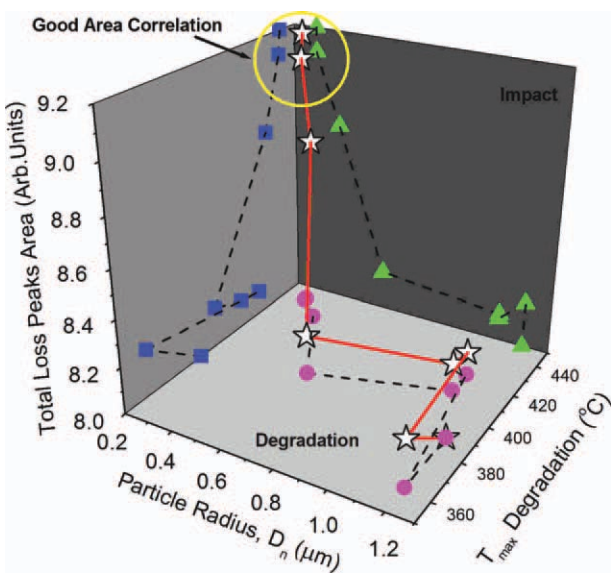

Figure 10 Interrelation of the morphological data with tan δ and TGA results for the PP/EVA blend-based nanocomposites. [Color figure can be viewed in the online issue, which is available at wileyonlinelibrary.com.]

CONCLUSIONS

In this study, the effects of the introduction of OMMT on the morphological, dynamic mechanical, and thermal properties of the PP/EVA blends were investigated. WAXS analysis showed that OMMT particles were mainly in an intercalated state in the blend-based nanocomposites. An analytical investigation with the TEM results and the calculated values of the interfacial tension and Δ_i showed that the OMMT nanoparticles were mainly localized in the EVA dispersed phase. SEM analysis revealed a significant reduction in the size and size distribution of the EVA domains with the introduction of OMMT nanoparticles. This refinement of domains was more pronounced in the presence of both OMMT and compatibilizer. DMA indicated that the incorporation of OMMT had a greater influence on the EVA phase than on PP. This was attributed to the selective localization of OMMT in the EVA phase. Investigation of loss peak area and storage modulus of the samples in terms of the O/C ratio revealed simultaneous enhancements in both the damping and storage modules with the incorporation of balanced amounts of OMMT and compatibilizer. The higher CID of the EVA domains was, the less obvious the supertoughening behavior was. The TGA results demonstrated that the addition of EVA to PP improved its thermal stability; this was more pronounced with the incorporation of OMMT. Also, the addition of PP-*g*-MA as a compatibilizer further enhanced the thermal stability because of its

compatibilization effect on the blend components and the induction of a better interaction between the OMMT platelets and the polymer pairs. The latter itself improved the dispersion state of the OMMT nanoparticles and intensified the char formation phenomenon. The correlation between the morphology, DMA, and TGA results showed that reduction of the EVA average domain size in the PP matrix enhanced both the thermal stability and toughness of the nanocomposites.

The authors thank Seyed Ali Monemian and Massude Khabaziyan for their helpful cooperation.

References

1. Soares, B. G.; Almeida, M. S. M.; Ranganathaiah, C.; Deepa Urs, M. V.; Siddaramaiah. Polym Test 2007, 26, 88.
2. Cook, R. F.; Koester, K. J.; Macosko, C. W.; Ajbani, M. Polym Eng Sci 2005, 45, 1487.
3. Li, Y.-Y.; Wang, Y.; Li, W.-Q.; Sheng, J. J Appl Polym Sci 2007, 103, 365.
4. Tang, L.; Qu, B.; Shen, X. J Appl Polym Sci 2004, 92, 3371.
5. Yang, J.; Zhang, Y.; Zhang, Y. Polymer 2003, 44, 5047.
6. McNally, T.; McShane, P.; Nally, G. M.; Murphy, W. R.; Cook, M.; Miller, A. Polymer 2002, 43, 3785.
7. Yang, H.; Zhang, X.; Qu, C.; Li, B.; Zhang, L.; Zhang, Q.; Fu, Q. Polymer 2007, 48, 860.
8. Thio, Y. S.; Argon, A. S.; Cohen, R. E.; Weinberg, M. Polymer 2002, 43, 3661.
9. Chan, C.-M.; Wu, J.; Li, J.-X.; Cheung, Y.-K. Polymer 2002, 43, 2981.
10. Lim, J.; Hassan, A.; Rahmat, A.; Wahit, M. U. Polym Int 2006, 55, 204.
11. Yu, Z.; Yin, J.; Yan, S.; Xie, Y.; Ma, J.; Chen, X. Polymer 2007, 48, 6439.
12. Si, M.; Araki, T.; Ade, H.; Kilcoyne, A. L. D.; Fisher, R.; Sokolov, J. C.; Rafailovich, M. H. Macromolecules 2006, 39, 4793.
13. Lipatov, Y. S.; Nesterov, A. E.; Ignatova, T. D.; Nesterov, D. A. Polymer 2002, 43, 875.
14. Lipatov, Y. S. Polymer 2002, 27, 1721.
15. Jang, B. N.; Wang, D.; Wilkie, C. A. Macromolecules 2005, 38, 6533.
16. Treece, M. A.; Oberhauser, J. P. Polymer 2007, 48, 1083.
17. Sun, T.; Dong, X.; Du, K.; Wang, K.; Fu, Q.; Han, C. C. Polymer 2008, 49, 588.
18. Martins, C. G.; Larocca, N. M.; Paul, D. R.; Peassan, L. A. Polymer 2009, 50, 1743.
19. Calcagno, C. I. W.; Mariani, C. M.; Teixeira, S. R.; Mauler, R. S. Compos Sci Tech 2008, 68, 2193.
20. Kusmono, Z. A.; Chow, W. S.; Takeichi, T. Eur Polym J 2008, 44, 1023.
21. Mehta, S.; Mirabella, F. M.; Rufener, K.; Bafna, A. J Appl Polym Sci 2004, 92, 928.
22. Goodarzi, V.; Jafari, S. H.; Khonakdar, H. A.; Monemian, S. A.; Hässler, R.; Jehnichen, D. J Polym Sci Part: B Polym Phys 2009, 47, 674.
23. Goodarzi, V.; Jafari, S. H.; Khonakdar, H. A.; Monemian, S. A.; Mortazavi, M. Polym Degrad Stab 2010, 95, 859.
24. Gopakumar, T. G.; Lee, J. A.; Kontopoulou, M.; Parent, J. S. Polymer 2002, 43, 5483.
25. Wu, S. Polymer 1985, 26, 1855.
26. Lee, K. Y.; Goettler, L. A. Polym Eng Sci 2004, 44, 1103.
27. Kawasumi, M.; Hasegawa, N.; Kato, M.; Usuki, A.; Okada, A. Macromolecules 1997, 30, 6333.
28. Tang, Y.; Hu, Y.; Wang, S.; Gui, Z.; Chen, Z.; Fan, W. J Appl Polym Sci 2003, 89, 2586.
29. As'Habi, L.; Jafari, S. H.; Baghaei, B.; Khonakdar, H. A.; Pötschke, P.; Böhme, F. Polymer 2008, 49, 2119.
30. Wu, S. J Macromol Sci Polym Rev 1974, 10, 1.
31. Guggenheim, E. A. J Chem Phys 1945, 13, 253.
32. Premphet, K.; Horanont, P. Polymer 2000, 41, 9283.
33. Lewin, M. Polym Adv Technol 2006, 17, 758.
34. Wu, S. Polymer Interface and Adhesion; Marcel Dekker: New York, 1982.
35. Wu, D.; Zhou, C.; Zhang, M. J Appl Polym Sci 2006, 102, 3628.
36. Fenouillot, F.; Cassagnau, P.; Majeste, J.-C. Polymer 2009, 50, 1333.
37. Liu, L.; Wang, Y.; Li, Y.; Wu, J.; Zhou, Z.; Jiang, C. Polymer 2009, 50, 3072.
38. Feng, M.; Gong, F.; Zhao, C.; Chen, G.; Zhang, S.; Yang, M. Polym Int 2004, 53, 1529.
39. Bagheri, R.; Pearson, R. A. Polymer 2000, 41, 269.
40. Gaymans, R. J. Toughening of Semicrystalline Thermoplastics; Wiley: New York, 2000.
41. Jafari, S. H.; Gupta, A. K. J Appl Polym Sci 2000, 78, 962.
42. Zhang, M.; Singh, R. M. Mater Lett 2004, 58, 408.
43. Lee, H.-S.; Fasulo, P. D.; Rodgers, W. R.; Paul, D. R. Polymer 2005, 46, 11673.
44. Sperling, L. H. Introduction to Physical Polymer Science; Wiley: Hoboken, NJ, 2006.
45. Jansen, P.; Soares, B. G. Polym Degrad Stab 1996, 52, 95.